The Edges of Hydrogen Terminated Graphene Ribbons

Energetics, Bandstructure and Magnetization

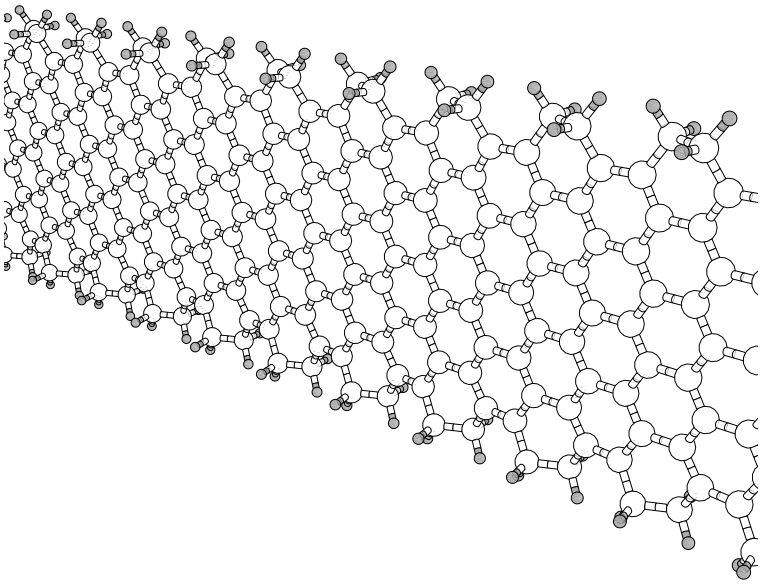

Tobias Wassmann

Master Thesis

Under the supervision of
Dr. Ari Seitsonen and Prof. Francesco Mauri
Institut de Minéralogie et de Physique des Milieux Condensés, Paris

Under the responsability of
Prof. Thomas Gehrmann
University of Zurich

Project coordination
Prof. Thomas Greber
University of Zurich

University of Zurich

April 11, 2008

Abstract

In this thesis we have examined the edges of hydrogen-terminated single-sheet graphene ribbons by means of *ab initio* density functional theory calculations. Edges in different crystal symmetry directions, with different planar reconstructions and different edge-hydrogen densities were considered. The studies concentrated on the analysis of the formation energy, the bandstructure and the magnetism of the ribbons. Following our primary goal, the identification of the energetically most favorable edge configuration under different chemical conditions, the formation energy was translated to a broad sector in thermodynamical phase space via the chemical potential of molecular hydrogen.

These considerations reveal that at room temperature and under ambient hydrogen pressure the monohydrogenated armchair ribbon represents the most stable configuration. In the area of negative formation energy where spontaneous breaking is possible, the dihydrogenated armchair ribbon becomes most favorable. None of the armchair ribbons analyzed in this study showed magnetism whereas zigzag ribbons can be magnetic or not depending on the edge configuration. The region where magnetism occurs, however could be reduced to low pressure, high temperature conditions.

The zero-point formation energies calculated here confirm our expectations based on the analysis of the Clar structures of the ribbons.

Contents

1 Preface

This thesis is the result of the studies I have performed in the last six months at the Institut de Minéralogie et de Physique des Milieux Condensés (IMPMC), Paris, in the group of Prof. Francesco Mauri and under the supervision of Dr. Ari Seitsonen. The formal aspect of the work is perhaps a little unusual for a Master-thesis and therefore deserves explanation.

At some point during the project, we realized that the accumulated results are worth a publication. Since the field is very competitive we decided—in agreement with all involved persons—to concentrate on the composition of a tentative draft of the planned article. The resulting manuscript consequentially represents the main part of the thesis and it is included in a separate document. Preliminary to that, I give a general introduction to the field on the next pages and include a chapter on the calculation methods.

In addition, a series of commented sketches, graphs and figures along the main lines of my work is presented in the appendix. This material can be seen as supporting and explanatory information for the paper. Unfortunately the time was too short to include a rigorous discussion of these things but I still wanted to include them and hope the reader can follow the outlined path.

I would like to thank Ari Seitsonen for the good cooperation, the support he gave me in all kinds of subjects and the time he took for this project in addition to his already tight schedule. It was a pleasure to work with you and you deserve much credit for the outcome of this work. I thank Prof. Francesco Mauri for giving me the chance to come to Paris and work under his excellent guidance. All group members, especially Michele Lazzeri and Marco Saitta deserve a big thank-you for the fruitful discussions and the engagement they brought to this project. I thank also Prof. Thomas Greber for the effort he made in organizing this thesis and his mentorship from which I benefited in the last two years. Not least, I would like to thank Prof. Thomas Gehrmann for the responsibility he took in representing this thesis in the faculty.

2 Introduction

Missing dimension in the carbon world. Carbon represents without any doubt one of the most intriguing elements, forming a vast amount of different allotropes with a wide range of physical properties. Besides the long known diamond and graphite structure, in the last 20 years mesoscopic carbon molecules like fullerenes [1] and nanotubes [2] attracted a lot of scientific and public interest. Due to their interesting dimensions, form factors, physical properties and sheer beauty, they constituted a whole new research area, that of mesoscopic carbon compounds, and raised a lot of hope for future applications.

At that point, however, the picture of carbon forms was incomplete from point of view of dimensionality [3,4]. While diamond and graphite represent 3D crystals, carbon nanotubes can be understood as 1D objects and the spherical fullerens as 0D. A two-dimensional form was missing.

Discovery of graphene. In 2004 a group around Novoselov and Geim from Manchester reported the production of atomically thin, isolated sheets of graphite [5]. This two-dimensional crystal, formed by carbon atoms arranged in a hexagonal honeycomb lattice, completed the picture and was given the name graphene.[1]

The early production techniques were astonishingly low-tech. By rubbing or repeated peeling with adhesive tape single sheets can be exfoliated from bulk graphite and then identified in optical microscopes. Despite its simplicity, this approach allows the production of large (up to 100 μm) high-quality samples [4] ready for experiments of various kinds.

Since then, graphene research formally took off. There are hundreds of scientific papers published every year on the subject, a peak is still out of sight, and one breathtaking result is hunting the other. Let us try to summarize some of the most remarkable ones.

Fundamental physics. Due to its unique electronic structure, graphene represents a perfect model system for quantum electrodynamics in condensed matter.[2] Its bandstructure exhibits two conical points in the reciprocal unit cell where the conduction band and the valence band meet, see Fig. 3 in the appendix. The electron energy in the neighborhood of these points depends linearly on the k-vector and leads to a light-like dispersion relation. Carrier transport is not described by the Schrödinger equation as

[1] The material, however, is not strictly two-dimensional. Either it is supported by a substrate and therefore part of a three-dimensional structure or, in its suspended form, shows surface roughening with out-of-plane deformations up to 1 nm [6].

[2] Actually this was recognized long before the discovery of graphene [7,8]. The material then was thought to be only an academic toy model though. But these studies certainly have been an inspiration for experiments, once the material was at hand.

in most condensed matter situations, but rather by a formal equivalent to the relativistic Dirac equation for massless particles [9]. Consequentially, charge carriers in graphene have an effective zero rest mass and travel at an effective 'speed of light' of $v_F = 10^6$ m/s [9].

Also following from the Dirac-like dynamics, graphene was theoretically predicted [10] and experimentally confirmed [11, 12] to show a distinctive half-integer form of the quantum Hall effect even at room temperature.

Another example of the insights graphene offers to fundamental physics will be given in one of the next issues of Science. It was demonstrated that the fine structure constant can not only be measured in sophisticated facilities and under special conditions but also in a table-top experiment by analyzing the light absorption of graphene [13].

Electronics. The importance of the material not only as playground for fundamental physics but also for technical applications was pointed out already when it was discovered [5]. Electrons and holes in graphene travel over long distances without scattering, resulting in ballistic transport on submicron distance under ambient conditions [14, 15]. Also spin transport over micrometer distances at room temperature was observed [16].

The conductivity in the material never falls below a minimum value, even in the limit of vanishing charge carrier concentrations [9]. And not at least, graphene's high electronic quality is expressed by a room temperature carrier mobility of $\sim 200\,000$ cm^2/V s what is by far higher than that of any other semiconductor [17].

All these properties make graphene a very promising material for future electronic devices.

Drawbacks. There are, however, some obstacles to overcome on the way to graphene based electronics. First of all, graphene represents a zero-gap semiconductor, making the material unsuitable for direct application in field effect transistors (FET) or other semiconductor devices [5].[3]

Carbon nanotubes (CNTs) on the other hand, have excellent properties for FET applications [18,19]. The periodic boundary conditions imposed by rolling a piece of graphene to the cylindrical form open up a band-gap in 2/3 of the cases (depending on the chirality of the tubes) [20–22]. Hence, a part of CNTs exhibit true semiconductor properties in addition to the electronic characteristics of graphene [23].

The problem with CNTs is that their chirality cannot be controlled during growth, making laborious separation procedures necessary. And the integration of CNTs in large scale electronic circuits represents another serious hurdle [24].

[3] Some prove-of-principle FET based on graphene have been studied. They exhibit only modest on/off resistance ratios [5].

Graphene Ribbons. In this context, graphene nanoribbons (GNRs) [25,26] appear as valuable alternative. The boundary conditions imposed on the material through confinement in one dimension can open up a bandgap as in the case of CNTs. GNRs therefore represent a perfect combination of graphene's advantageous electronic properties and the semiconductor characteristics of CNT [27,28], but offering in addition the possibility of lithographic patterning [29,30].

The vast amount of scientific interest paid to GNRs in the last few years, however, is not only owed to their formidable applicability in semiconductor devices, but also to the fact that they represent models to study the edges of graphene and how they influence the properties of the material.

Edges. GNRs appear in two fundamental edge topologies, armchair (AGNRs) and zigzag (ZGNRs), see Fig. 4 in the appendix. Mixtures are also possible. Based on theoretical considerations, it was found that ZGNRs feature a spin-polarizied state localized at the edges [31]. In the ground-state, the net-polarization at the two edges is of opposite sign. The energies of these spin-polarized states can be shifted by applying external fields, resulting in metallic conduction for one spin orientation and isolation for the other (so-called half-metalicity) [32]. Such properties are very rare and make ZGNRs a sought-after candidate for spintronic devices.

The width of the GNRs [30], their edge topology [25] and decoration [33], however, have a big influence on the electronic properties. In particular, an inverse power law was found to describe the decrease of the bandgap as a function of increasing ribbon widths [34]. Thus, for semiconductor applications, very narrow ribbons are necessary.

Using lithographic techniques, the production of GNRs as narrow as 20 nm has been reported [29,30]. Further minimization seems difficult at the moment and the edges produced in this way show high disorder. In a recently published chemical derivation, GNRs with very smooth and well defined edges and widths down to sub 10 nm could be realized [35].

The exact geometry and edge decoration of the GNRs produced in this attempt, however, are not known.

Goal of this thesis. Using density functional theory (DFT) calculations we want to find the most stable configuration of hydrogen-terminated GNRs. To this end we perform a systematic study of different edge geometries, reconstructions and edge-hydrogen densities.

We are aware of the fact, that under different chemical conditions the most stable structure will vary and that DFT calculations are only valid at the absolute zero point. By expressing the formation energy of the GNRs as a function of the hydrogen chemical potential we expand the analysis of their relative stability to the whole thermodynamic phase space.

This analysis gives a prediction of the edge configuration and electronic properties of GNRs chemically produced in a hydrogen dominated environment. If one day cutting of graphene into ribbons with atomically defined edges will be possible, we can predict what hydrogen-decoration is most probable. The corresponding studies for other elements than hydrogen will follow.

Part of the motivation was also to investigate under what conditions the much discussed magnetic, monoydrogenated ZGNR is favorable. Based on calculations at the absolute zero point and the observation that the giant benzenoid hydrocarbons described lately [36] have mainly armchair edges, we have some doubts concerning the stability of this structrue.

Armchair edges are more stable because they interfere less with the intrinsic aromaticity of graphene sheets. Usual zigzag edges suppress the aromaticity as an analysis of their Clar structures shows, see Fig. 6. However, we found a zigzag edge with a particular edge-hydrogen termination that does not destroy the aromaticity. The analysis showed that this structure indeed represents the most favorable configuration in a small region of phase space, but exhibits no magnetization.

3 Density functional theory

All calculations in this thesis were performed within density functional theory (DFT). The DFT framework has been established in physics and chemistry to calculate properties of large quantum mechanical systems and I have already given a short overview of its fundamental aspects in my Bachelor thesis [37] (based on [38]). After a short summary of these concepts, here I also go into some more advanced subjects.

Outline. A quantum mechanical system and all its properties are described by the corresponding wave function $\psi(\vec{r}, \vec{r}_2, \ldots, \vec{r}_N)$. Solving the many particle Schrödinger equation for a big system directly in order to obtain the required information is an attempt with less prospect to success. Most problems are not solvable analytically and the Schrödinger equation is too expensive to solve numerically in terms of calculation time and data storage. DFT represents a way to obtain all the required information (at least about the ground state) much more elegantly.

First Hohenberg-Kohn theorem. First of all, in DFT, normally only the electrons are treated quantum mechanically, the atomic nuclei are only represented by the potential $v(\vec{r})$ that they impose on the electrons. Then the focus is shifted from the many particle wave function to the electron density

$$n(\vec{r}) = N \int \mathrm{d}^3 r_2 \ldots \mathrm{d}^3 r_N \; \psi^*(\vec{r}, \vec{r}_2, \ldots, \vec{r}_N)\, \psi(\vec{r}, \vec{r}_2, \ldots, \vec{r}_N)\,. \tag{1}$$

In fact, for the ground state, the electron density $n_0(\vec{r})$ is equivalent to the many body wave function $\psi_0(\vec{r}_1, \ldots, \vec{r}_N)$. The first Hohenberg-Kohn theorem namely states, that the ground state electron density $n_0(\vec{r})$ of a many electron system in the presence of an external potential $v(\vec{r})$ uniquely determines this external potential (up to an additive constant) [39]. Through the Schrödinger equation

$$\left(-\frac{\hbar^2}{2m} \sum_{i=1}^{N} \nabla_i^2 + V_{\mathrm{ext}} + U \right) \psi = E\psi\,. \tag{2}$$

then the wave function can be obtained in principle.

Energy functional. Put in other words, the wave function corresponding to a given ground state density is that one which reproduces the density via (1) and minimizes the energy

$$E[\psi] = \langle \psi | T + V_{\mathrm{ext}} + U | \psi \rangle\,. \tag{3}$$

In eqs. (2) and (3), V_{ext} denotes the external potential imposed by the atomic nuclei

$$V_{\text{ext}} = \sum_{i}^{N} v(\vec{r}_i) = -\sum_{k,i} \frac{Z_k e^2}{|\vec{r} - \vec{R}_k|}\,,$$

and U the Coulomb interaction between the electrons

$$U = \sum_{i<j} \frac{e^2}{|\vec{r}_i - \vec{r}_j|}\,.$$

Second Hohenberg-Kohn theorem. The second Hohenberg-Kohn theorem states, that for a given external potential $v(\vec{r})$, also an energy functional of the density, $E_v[n]$, exists that assumes its minimum for the correct ground state density $n_0(\vec{r})$. For instance, the energy in the external potential can easily be written as

$$E_{\text{ext}}[n] = \int \mathrm{d}^3 r\, n(\vec{r})\, v(\vec{r})$$

but also the kinetic energy T and the electron-electron interaction energy E_{int} in

$$E_v[n] = T[n] + E_{\text{int}}[n] + E_{\text{ext}}[n] \tag{4}$$

can be thought of as functionals of the density. The way DFT works, is clear. An initial external potential is set up based on the coordinates of the atomic nuclei and their atomic number. Then by minimizing the total energy functional (4), the corresponding ground state density is found. This density gives rise for a new external potential via the first Hohenberg-Kohn theorem and so on. The process is iterated until self-consistency is achieved.

Kohn-Sham approach. In the Kohn-Sham approach [40], minimization of the total energy functional (4) is done by introducing a set of N non-interacting single particle wave functions $\phi_i(\vec{r})$ with the same density

$$n_{\text{s}}(\vec{r}) = \sum_{i=1}^{N} |\phi_i(\vec{r})|^2 \tag{5}$$

as the original interactive system. The kinetic energy of the auxiliary system expressed in terms of the single-particle orbitals reads

$$T_{\text{s}} = -\frac{\hbar^2}{2m} \sum_{i=1}^{N} \int \mathrm{d}^3 r\, \phi_i^*(\vec{r})\, \nabla^2 \phi_i(\vec{r})\,. \tag{6}$$

Remark that this is an implicit functional of the density n because the Kohn-Sham orbitals $\phi_i(\vec{r})$ are functionals of the density as the first Hohenberg-Kohn theorem shows.

Hartree energy. The Coulomb part of the electron-electron interaction can be taken into account by introducing the Hartree potential

$$v_{\mathrm{H}}(\vec{r}) = e^2 \int \mathrm{d}^3 r' \, \frac{n(\vec{r}')}{|\vec{r} - \vec{r}'|} \tag{7}$$

and the corresponding Hartree energy

$$E_{\mathrm{H}}[n] = \frac{1}{2} \int \mathrm{d}^3 r \, n(\vec{r}) \, v_{\mathrm{H}}(\vec{r}) = \frac{e^2}{2} \iint \mathrm{d}^3 r \, \mathrm{d}^3 r' \, \frac{n(\vec{r}) n(\vec{r}')}{|\vec{r} - \vec{r}'|} \, .$$

The difference between the kinetic energy of the interacting system and the auxiliary system as well as all contributions to the electron-electron interaction other than the Hartree energy are summarized in the exchange correlation energy

$$E_{\mathrm{xc}} = (T - T_{\mathrm{s}}) + (E_{\mathrm{int}} - E_{\mathrm{H}}) \, .$$

This quantity consists of the exchange energy due to the Pauli exclusion principle and the fermionic correlation contributions. With that, we can rewrite the total energy functional as

$$E_v[n] \quad = \quad T_{\mathrm{s}}[n] + E_{\mathrm{H}}[n] + E_{\mathrm{xc}}[n] + E_{\mathrm{ext}}[n] \, . \tag{8}$$

This equation is exact, there is no term left out and no approximation has been made. However, no exact form of $E_{\mathrm{xc}}[n]$ is known, so for this term an approximation has to be introduced.

Kohn-Sham equations. Minimization of the total energy functional (8) is performed via the variation principle. Since the kinetic energy T_{s} is given as a functional of the Kohn-Sham orbitals, variation is taken not with respect to the density n but to $\phi_i^*(\vec{r})$. The constraints that the orbitals are orthonormal, $\langle \phi_i | \phi_j \rangle = \delta_{ij}$, and that the number of electrons is conserved, $N = \int n(\vec{r}) \mathrm{d}^3 r$, are implemented by introducing a Lagrange multiplier term:

$$\begin{aligned}
0 \quad &= \quad \frac{\delta}{\delta \phi_i^*(\vec{r})} \Big[E_v[n] - \sum_{l,k}^{N} \epsilon_{lk} \Big(\int \phi_l^*(\vec{r'}) \phi_k(\vec{r'}) \mathrm{d}^3 r' - \delta_{lk} \Big) \Big] \\
&= \quad \frac{\delta \, E_v[n]}{\delta \phi_i^*(\vec{r})} - \epsilon_i \phi_i(\vec{r}) \qquad \text{with } \epsilon_i = \epsilon_{ii} \\
&= \quad \frac{\delta \, T_s[n]}{\delta \phi_i^*(\vec{r})} + \left[\frac{\delta \, E_{\mathrm{H}}[n]}{\delta n(\vec{r})} + \frac{\delta \, E_{\mathrm{xc}}[n]}{\delta n(\vec{r})} + \frac{\delta \, E_{\mathrm{ext}}[n]}{\delta n(\vec{r})} \right] \frac{\delta \, n(\vec{r})}{\delta \phi_i^*(\vec{r})} - \epsilon_i \phi_i(\vec{r}) \\
&= \quad -\frac{\hbar^2 \nabla^2}{2m} \phi_i(\vec{r}) + \big[v_{\mathrm{H}}(\vec{r}) + v_{\mathrm{xc}}(\vec{r}) + v(\vec{r}) \big] \phi_i(\vec{r}) - \epsilon_i \phi_i(\vec{r}) \, .
\end{aligned}$$

This leads to the famous Kohn-Sham equations

$$\left[-\frac{\hbar^2 \nabla^2}{2m} + v_{\mathrm{s}}(\vec{r}) \right] \phi_i(\vec{r}) = \epsilon_i \phi_i(\vec{r}) \, , \tag{9}$$

with the effective potential

$$v_{\mathrm{s}} = v + v_{\mathrm{H}} + v_{\mathrm{xc}}\,. \tag{10}$$

The potential $v_{\mathrm{xc}}(\vec{r}) = \frac{\delta E_{\mathrm{xc}}[n]}{\delta n(\vec{r})}$ for the exchange correlation energy can only be calculated if an approximation for E_{xc} has been chosen.

To sum things up, in this approach we have substituted the task of solving the many-body Schrödinger equation by minimizing $E_v[n]$, and the minimization of $E_v[n]$ by solving the Schrödinger-like equations of a non-interacting system.

The exchange correlation energy. In the construction of the total energy functional (8), we have separated the known and easy to compute contributions from the complicated many-body effects in E_{xc}. For this term then an approximation has to be choosen, what of course is only justified if its contribution is small compared to the others.

Our ignorance of the exact form of E_{xc}, however, is not the only reason for the approximative approach to this quantity. In fact, some contributions to E_{xc}, are known exactly. For instance the exchange energy can be written in terms of the Kohn-Sham orbitals as

$$E_{\mathrm{x}} = -\frac{e^2}{2} \sum_{j,k} \int \mathrm{d}^3 r \int \mathrm{d}^3 r' \, \frac{\phi_j^*(\vec{r})\phi_k^*(\vec{r}')\phi_j(\vec{r})\phi_k(\vec{r})}{|\vec{r} - \vec{r}'|}\,. \tag{11}$$

So, the part which has to be approximated could be further reduced. This, however, is usually not done in DFT calculations. The evaluation of (11) is an extremely expensive computational tasks and in addition, the all in all accuracy is higher if an approximation for the whole E_{xc} is taken due to error cancelation.

For the precise form of E_{xc}, different approaches are in use. In the localized density approximation (LDA), E_{xc} is given in a form that depends only on the local density:

$$E_{\mathrm{xc}}^{\mathrm{LDA}}[n] = \int \mathrm{d}^3 r \, e_{\mathrm{xc}}(n(\vec{r}))\,.$$

In the generalized-gradient approximation (GGA) also a dependence on the variation of the density is allowed, leading to an expression of the form

$$E_{\mathrm{xc}}^{\mathrm{GGA}}[n] = \int \mathrm{d}^3 r \, f(n, \nabla n)\,. \tag{12}$$

For the function $f(n, \nabla n)$, very different choices exist, constructed for example by fitting a parametrized expression to some test sets.

Spin-polarization. The formulation of DFT presented up to this point concentrates on the particle or charge density $n(\vec{r})$ and can be considered as *charge-only* theory. Often an extension called *spin*-DFT (SDFT) is used that employs one density for each spin, $n_\uparrow(\vec{r})$ and $n_\downarrow(\vec{r})$. This modification of the theory allows the study of states with internal magnetization and properties in the presence of an external magnetic field.

The formulation of SDFT is essentially the same as presented above with an additional index for the spin. The total particle density is

$$n(\vec{r}) = n_\uparrow(\vec{r}) + n_\downarrow(\vec{r})$$

and the spin-magnetization density reads

$$m(\vec{r}) = \mu_0 \left(n_\uparrow(\vec{r}) - n_\downarrow(\vec{r})\right)$$

with the Bohr magneton μ_0. In the Kohn-Sham equations,

$$\left[-\frac{\hbar^2\nabla^2}{2m} + v_{\mathrm{s},\sigma}(\vec{r})\right] \phi_{i,\sigma}(\vec{r}) = \epsilon_{i,\sigma}\phi_{i,\sigma}(\vec{r})\,,$$

two different effective potentials, $v_{\mathrm{s},\sigma}(\vec{r}) = v_\sigma(\vec{r}) + v_{\mathrm{H}}(\vec{r}) + v_{\mathrm{xc},\sigma}(\vec{r})$, have to be applied. The potential in the presence of an external magnetic field depends on the spin and changes to $v_\sigma(\vec{r}) = v(\vec{r}) - \sigma\mu_0 B$ (with $\sigma = \pm 1$). In any case, the exchange correlation energy will depend on both spin-densities, so for the corresponding potential holds

$$v_{\mathrm{xc},\sigma}(\vec{r}) = \frac{\delta E_{\mathrm{xc}}^{\mathrm{SDFT}}[n_\uparrow, n_\downarrow]}{\delta n_\sigma(\vec{r})}\,.$$

The internal magnetic field B_{xc} in spin-polarized systems is then given by $v_{\mathrm{xc},\downarrow} - v_{\mathrm{xc},\uparrow} = \mu_0 B_{\mathrm{xc}}$.

Plane waves. Besides the approximative treatment of E_{xc} discussed above, there is another approximation in the way, the Kohn-Sham equations (9) are numerically solved. This is done by expanding the Kohn-Sham orbitals ϕ_i in an appropriate set of basis functions and solve for the corresponding coefficients in the expansion.

A priori, these equations have to be solved for all electrons in the configuration, what can be infinitely many in cases like our infinite ribbons. If the system is periodic, however, according to the Bloch theorem, it is sufficient to consider the electrons in a periodic cell. Each wave vector component of these finitely many wave functions can then be written as a product of a cell-periodic part and a plain wave part [41, 42],

$$\phi_{i,\vec{k}}(\vec{r}) = u_{i,\vec{k}}(\vec{r})\, \exp(i\vec{k}\cdot\vec{r})\,,$$

where the wave vector $\vec{k}$ can be assumed to lie in the first Brillouin zone. The cell periodic part $u_{i,\vec{k}}(\vec{r})$ has the same periodicity as the lattice. It can therefore be expanded in plane waves whose wave vectors $\vec{G}$ are reciprocal lattice vectors

$$u_{i,\vec{k}}(\vec{r}) = \sum_{\vec{G}} c_{i,\vec{k}+\vec{G}} \, \exp(i\vec{G}\cdot\vec{r}) \, .$$

So, in the end each wave function can be written as sum of plane waves[4]

$$\phi_i(\vec{r}) \;\; = \;\; \sum_{\vec{k}} \sum_{\vec{G}} c_{i,\vec{k}+\vec{G}} \, \exp\left(i(\vec{G}+\vec{k})\cdot\vec{r}\right) . \tag{13}$$

This a double infinite sum over all the discrete reciprocal lattice vectors, $\vec{G}$, and the continuous vectors in the first Brillouin zone, $\vec{k}$. In practical calculations only plane waves whose kinetic energy is smaller than some particular cutoff energy, E_{cutoff}, are used [41]:

$$\frac{\hbar^2 \, |\vec{k}+\vec{G}|^2}{2\,m} < E_{\text{cutoff}} \, . \tag{14}$$

The coefficients for the plane waves with higher kinetic energy are typically less important. Furthermore, experience shows that the sum (or better the integral) over $\vec{k}$ can be approximated very accurately by a sum over an affordable number of k-points [41, 43]. This restriction together with the condition (14) makes the summation in (13) finite and numerically accessible.

The accuracy of the calculation can always be improved by using more k-points and a higher cutoff energy. These two are the most important convergence parameters in DFT calculations. See our convergence tests in Figs. 7–11.

Pseudopotentials. The chemical bonding and solid-state properties of any system are mainly determined by the valence electrons. The core electrons of an atom, on the other hand, remain nearly unchanged, no matter in what environment the atom is put. Based on this fact, it is the goal of the pseudopotential approach in DFT to reduce the numeric effort by excluding the core electrons from the self-consistent calculation.

This not only cuts the number of electrons considered, but also makes the calculation of the remaining valence electrons less extensive. The valence orbitals namely oscillate rapidly in the region of the atom core to assure orthogonality to the orbitals of the core electrons. It requires a huge number of plane waves in the basis set to account for these oscillations [38].

The idea behind the approach is to replace the ionic potential v and the core electrons by a pseudopotential v^{pp}, such that outside a radius r_{c}

[4] There exist also other suitable basis sets [38].

separating the core form the valence region, the valence orbitals calculated in v^{PP} are identical to the ones calculated in v [41]. Ideally, the valence orbitals in the pseudopotential have no root in in the core region, making it possible to expand them in a much smaller plane wave basis set than the original valence orbitals.

The density of the core electrons and the pseudopotential v^{PP} are determined in preliminary Kohn-Sham calculations on reference systems. The way v^{PP} is constructed, however, is not unique and various conceptions are in use [44].

DFT and thermodynamics. The relative stability of GNR with different edges is analyzed by adopting methods used in surface science [45, 46]. The quantity that is compared is called edge energy or edge free energy.[5] We define it in analogy to the surface free energy as

$$E_{\mathrm{edge}}(T, p_{\mathrm{H_2}}, p_{\mathrm{tot}}) = \frac{1}{2\, l_{\mathrm{cell}}} \Big(G_{\mathrm{ribbon}}(T, p_{\mathrm{tot}}) - n_{\mathrm{C}}\, \mu_{\mathrm{C}}(T, p_{\mathrm{tot}}) - n_{\mathrm{H}}\, \frac{\mu_{\mathrm{H_2}}(T, p_{\mathrm{H_2}})}{2} \Big) .$$

Here l_{cell} denotes the edge length of the unit cell. The factor 2 accounts for the two edges on both sides of the ribbon. G_{ribbon} is the Gibbs free energy per unit cell of the ribbon and n_{C} and n_{H} are respectively the number of carbon and hydrogen atoms in the ribbon. $p_{\mathrm{H_2}}$ is the partial pressure of $\mathrm{H_2}$ and p_{tot} the total pressure of the system. μ_{C} and $\mu_{\mathrm{H_2}}$ represent the chemical potentials for hydrogen and carbon.

We assumed that bulk graphene is in equilibrium with carbon in its natural state,

$$G_{\mathrm{bulk}}(T, p_{\mathrm{tot}}) = n\, \mu_{\mathrm{C}}(T, p_{\mathrm{tot}}) ,$$

where G_{bulk} is the Gibbs free energy per unit cell of a graphene sheet and n the number of carbon atoms per unit cell. In the primitive hexagonal unit cell, $n = 2$ holds. Thus, we can rewrite the edge energy as

$$E_{\mathrm{edge}}(T, p_{\mathrm{H_2}}, p_{\mathrm{tot}}) = \frac{1}{2\, l_{\mathrm{cell}}} \Big(G_{\mathrm{ribbon}}(T, p_{\mathrm{tot}}) - n_{\mathrm{C}}\, \frac{G_{\mathrm{bulk}}(T, p_{\mathrm{tot}})}{2} - n_{\mathrm{H}}\, \frac{\mu_{\mathrm{H_2}}(T, p_{\mathrm{H_2}})}{2} \Big) .$$

This formula gives E_{edge} in the energy gauge of classical thermodynamics where the formation energy of an element at standard conditions is zero. We want to convert it to the DFT gauge, such that G_{ribbon} and G_{bulk} just represent the DFT total energies. In the DFT gauge, we then have

$$E_{\mathrm{edge}}(T, p_{\mathrm{H_2}}) = \frac{1}{2\, l_{\mathrm{cell}}} \Big(E_{\mathrm{ribbon}} - n_{\mathrm{C}}\, \frac{E_{\mathrm{bulk}}}{2} - n_{\mathrm{H}}\, \frac{\mu_{\mathrm{H_2}}(T, p_{\mathrm{H_2}})}{2} \Big) ,$$

which is already enough to compare relative stabilities by plotting E_{edge} versus $\mu_{\mathrm{H_2}}$. However, if we want to assign temperature and pressure values to E_{edge} we have to transpose also $\mu_{\mathrm{H_2}}$ to the DFT energy scale.

[5] In our discussions we used the terms 'edge free energy', 'edge energy' and '(edge) formation energy' as synonyms.

In the ideal gas approximation, the hydrogen chemical potential can be written as

$$\mu_{\mathrm{H_2}}(T, p_{\mathrm{H_2}}) = \mu_{\mathrm{H_2}}(T, p^0_{\mathrm{H_2}}) + \frac{1}{2}\, kT\, \ln\left(\frac{p_{\mathrm{H_2}}}{p^0_{\mathrm{H_2}}}\right). \tag{15}$$

For a better understanding of the path in the phase space, we want to reformulate this by introducing a term for the change in the chemical potential when moving from $T = 0$ to $T = T$ at constant pressure $p^0_{\mathrm{H_2}}$:

$$\Delta\mu_{\mathrm{H_2}}(p_{\mathrm{H_2}})|^{T=T}_{T=0} = \mu_{\mathrm{H_2}}(T, p^0_{\mathrm{H_2}}) - \mu_{\mathrm{H_2}}(0, p^0_{\mathrm{H_2}}) \tag{16}$$

Combining eq. (15) and (16), we obtain

$$\mu_{\mathrm{H_2}}(T, p_{\mathrm{H_2}}) = \mu_{\mathrm{H_2}}(0, p^0_{\mathrm{H_2}}) + \Delta\mu_{\mathrm{H_2}}(p^0_{\mathrm{H_2}})|^{T=T}_{T=0} + \frac{1}{2}\, kT\, \ln\left(\frac{p_{\mathrm{H_2}}}{p^0_{\mathrm{H_2}}}\right). \tag{17}$$

The value for $\Delta\mu_{\mathrm{H_2}}(p_{\mathrm{H_2}})|^{T=T}_{T=0}$ can be deduced from thermodynamic tables [47].

Now we can define the chemical potential on the DFT energy scale in analogy to eq. (17) as

$$\mu'_{\mathrm{H_2}}(T, p_{\mathrm{H_2}}) = E^{\mathrm{DFT}}_{\mathrm{H_2}} + \Delta\mu_{\mathrm{H_2}}(p^0_{\mathrm{H_2}})|^{T=T}_{T=0} + \frac{1}{2}\, kT\, \ln\left(\frac{p_{\mathrm{H_2}}}{p^0_{\mathrm{H_2}}}\right).$$

This expression allows us to translate the chemical potential to temperature and pressure conditions and vice versa. Note that at absolute zero temperature $\mu'_{\mathrm{H_2}} = E^{\mathrm{DFT}}_{\mathrm{H_2}}$.

References

[1] H. W. Kroto, J. R. Heath, S. C. O'Brien, R. F. Curl, and R. E. Smalley. C_{60}: Buckminsterfullerene. *Nature*, 318(6042):162–163, 1985.

[2] S. Iijima. Helical microtubules of graphitic carbon. *Nature*, 354(6348):56–58, 1991.

[3] A. K. Geim and K. S. Novoselov. The rise of graphene. *Nature Mater*, 6(3):183–191, 2007.

[4] K. S. Novoselov, S. V. Morozov, T. M. G. Mohinddin, L. A. Ponomarenko, D. C. Elias, R. Yang, I. I. Barbolina, P. Blake, T. J. Booth, D. Jiang, J. Giesbers, E. W. Hill, and A. K. Geim. Electronic properties of graphene. *Phys. Stat. Sol. (b)*, 244(11):4106–4111, 2007.

[5] K. S. Novoselov, A. K. Geim, S. V. Morozov, D. Jiang, Y. Zhang, S. V. Dubonos, I. V. Grigorieva, and A. A. Firsov. Electric Field Effect in Atomically Thin Carbon Films. *Science*, 306(5696):666–669, 2004.

[6] J. C. Meyer, A. K. Geim, M. I. Katsnelson, K. S. Novoselov, T. J. Booth, and S. Roth. The structure of suspended graphene sheets. *Nature*, 446(7131):60–63, 2007.

[7] G. W. Semenoff. Condensed-Matter Simulation of a Three-Dimensional Anomaly. *Phys. Rev. Lett.*, 53(26):2449–2452, 1984.

[8] F. D. M. Haldane. Model for a Quantum Hall Effect without Landau Levels: Condensed-Matter Realization of the "Parity Anomaly". *Phys. Rev. Lett.*, 61(18):2015–2018, 1988.

[9] K. S. Novoselov, A. K. Geim, S. V. Morozov, D. Jiang, M. I. Katsnelson, I. V. Grigorieva, S. V. Dubonos, and A. A. Firsov. Two-dimensional gas of massless Dirac fermions in graphene. *Nature*, 438(7065):197–200, 2005.

[10] V. P. Gusynin and S. G. Sharapov. Unconventional Integer Quantum Hall Effect in Graphene. *Phys. Rev. Lett.*, 95(14):146801, 2005.

[11] K. S. Novoselov, Z. Jiang, Y. Zhang, S. V. Morozov, H. L. Stormer, U. Zeitler, J. C. Maan, G. S. Boebinger, P. Kim, and A. K. Geim. Room-Temperature Quantum Hall Effect in Graphene. *Science*, 315(5817):1379–, 2007.

[12] Y. Zhang, Y.-W. Tan, H. L. Stormer, and Ph. Kim. Experimental observation of the quantum Hall effect and Berry's phase in graphene. *Nature*, 438(7065):201–204, 2005.

[13] R. R. Nair, P. Blake, A. N. Grigorenko, K. S. Novoselov, T. J. Booth, T. Stauber, N. M. R. Peres, and A. K. Geim. Fine Structure Constant Defines Visual Transparency of Graphene. *Science*, 2008. DOI: 10.1126/science.1156965.

[14] F. Miao, S. Wijeratne, Y. Zhang, U. C. Coskun, W. Bao, and C. N. Lau. Phase-Coherent Transport in Graphene Quantum Billiards. *Science*, 317(5844):1530–1533, 2007.

[15] A. H. Castro Neto, F. Guinea, N. M. R. Peres, K. S. Novoselov, and A. K. Geim. The electronic properties of graphene. arXiv.org:0709.1163, 2007.

[16] N. Tombros, C. Jozsa, M. Popinciuc, H. T. Jonkman, and B. J. van Wees. Electronic spin transport and spin precession in single graphene layers at room temperature. *Nature*, 448(7153):571–574, 2007.

[17] S. V. Morozov, K. S. Novoselov, M. I. Katsnelson, F. Schedin, D. C. Elias, J. A. Jaszczak, and A. K. Geim. Giant Intrinsic Carrier Mobilities in Graphene and Its Bilayer. *Phys. Rev. Lett.*, 100(1):016602, 2008.

[18] S.J. Tans, A. R. M. Verschueren, and C. Dekker. Room-temperature transistor based on a single carbon nanotube. *Nature*, 393(6680):49–52, 1998.

[19] Phaedon Avouris. Molecular Electronics with Carbon Nanotubes. *Acc. Chem. Res.*, 35:1026–1034, 2002.

[20] N. Hamada, S. Sawada, and A. Oshiyama. New one-dimensional conductors: Graphitic microtubules. *Phys. Rev. Lett.*, 68(10):1579–1581, 1992.

[21] R. Saito, M. Fujita, G. Dresselhaus, and M. S Dresselhaus. Electronic structure of chiral graphene tubules. *Appl. Phys. Lett.*, 60(18):2204–2206, 1992.

[22] M. S. Arnold, A. A. Green, J. F. Hulvat, S. I. Stupp, and M. C. Hersam. Sorting carbon nanotubes by electronic structure using density differentiation. *Nature Nano*, 1(1):60–65, 2006.

[23] St. Frank, Ph. Poncharal, Z. L. Wang, and W. A. Heer. Carbon Nanotube Quantum Resistors. *Science*, 280(5370):1744–1746, 1998.

[24] P.L. McEuen, M.S. Fuhrer, and H. Park. Single-walled carbon nanotube electronics. *IEEE Trans. Nanotechnol.*, 1(1):78–85, 2002.

[25] K. Nakada, M. Fujita, G. Dresselhaus, and M. S. Dresselhaus. Edge state in graphene ribbons: Nanometer size effect and edge shape dependence. *Phys. Rev. B*, 54(24):17954–17961, 1996.

[26] C. Berger, Z. Song, X. Li, X. Wu, N. Brown, C. Naud, D. Mayou, T. Li, J. Hass, A. N. Marchenkov, E. H. Conrad, Ph. N. First, and W. A. de Heer. Electronic Confinement and Coherence in Patterned Epitaxial Graphene. *Science*, 312(5777):1191–1196, 2006.

[27] B. Obradovic, R. Kotlyar, F. Heinz, P. Matagne, T. Rakshit, M. D. Giles, M. A. Stettler, and D. E. Nikonov. Analysis of graphene nanoribbons as a channel material for field-effect transistors. *Appl. Phys. Lett.*, 88(14):142102, 2006.

[28] Z. Xu, Q.-S. Zheng, and G. Chen. Elementary building blocks of graphene-nanoribbon-based electronic devices. *Appl. Phys. Lett.*, 90(22):223115, 2007.

[29] C. Berger, Z. Song, T. Li, X. Li, A.Y. Ogbazghi, R. Feng, Z. Dai, A.N. Marchenkov, E.H. Conrad, P.N. First, and W.A. deHeer. Ultrathin Epitaxial Graphite: 2D Electron Gas Properties and a Route toward Graphene-based Nanoelectronics. *J. Phys. Chem. B*, 108(52):19912–19916, 2004.

[30] M. Y. Han, B. Özyilmaz, Y-Zhang, and Ph. Kim. Energy Band-Gap Engineering of Graphene Nanoribbons. *Phys. Rev. Lett.*, 98(20):206805, 2007.

[31] A. Yamashiro, Y. Shimoi, K. Harigaya, and K. Wakabayashi. Spin- and charge-polarized states in nanographene ribbons with zigzag edges. *Phys. Rev. B*, 68(19):193410, 2003.

[32] Y.-W. Son, M. L. Cohen, and St. G. Louie. Half-metallic graphene nanoribbons. *Nature*, 444(7117):347–349, 2006.

[33] D. Gunlycke, J. Li, J. W. Mintmire, and C. T. White. Altering low-bias transport in zigzag-edge graphene nanostrips with edge chemistry. *Appl. Phys. Lett.*, 91(11):112108, 2007.

[34] V. Barone, O. Hod, and G.E. Scuseria. Electronic structure and stability of semiconducting graphene nanoribbons. *Nano Lett.*, 6(12):2748–2754, 2006.

[35] X. Li, X. Wang, L. Zhang, S. Lee, and H. Dai. Chemically Derived, Ultrasmooth Graphene Nanoribbon Semiconductors. *Science*, 319(5867):1229–1232, 2008.

[36] M.D. Watson, A. Fechtenkotter, and K. Mullen. Big Is Beautiful-"Aromaticity" Revisited from the Viewpoint of Macromolecular and Supramolecular Benzene Chemistry. *Chem. Rev.*, 101(5):1267–1300, 2001.

[37] T. Wassmann. The Electronic Structure and Quantum Dynamics of $H_2@C_{60}$. Bachelor Thesis, University of Zurich, 2007.

[38] Klaus Capelle. A bird's-eye view of density-functional theory, 2002. arXiv.org:cond-mat/0211443.

[39] P. Hohenberg and W. Kohn. Inhomogeneous Electron Gas. *Phys. Rev. B.*, 136:864–871, 1964.

[40] W. Kohn and L. J. Sham. Self-Consistent Equations Including Exchange and Correlation Effects. *Phys. Rev. A*, 140(4):1133–1138, 1965.

[41] M. C. Payne, M. P. Teter, D. C. Allan, T. A. Arias, and J. D. Joannopoulos. Iterative minimization techniques for ab initio total-energy calculations: molecular dynamics and conjugate gradients. *Rev. Mod. Phys.*, 64(4):1045–1097, 1992.

[42] Ch. Kittel. *Einfhrung in die Festkrperphysik.* Oldenbourg, München, 2006.

[43] P. Giannozzi. Metodi Numerici in Struttura Elettronica, 2006. http://www.fisica.uniud.it/∼giannozz/Corsi/metnum.html.

[44] D. Porezag, M. R. Pederson, and A. Y. Liu. The Accuracy of the Pseudopotential Approximation within Density-Functional Theory. *Phys. Stat. Sol. (b)*, 217(1):219–230, 2000.

[45] CL Bailey, A Wander, S Mukhopadhyay, BG Searle, and NM Harrison. Ab initio surface thermodynamics in multi component environments, 2007. http://www.scientificcommons.org/23406578.

[46] K. Reuter and M. Scheffler. Composition, structure, and stability of $RuO_2(110)$ as a function of oxygen pressure. *Phys. Rev. B*, 65(3):035406, 2001.

[47] M. W. Chase, C. A. Davies, J. R. Downey, D. J. Frurip, R. A. McDonald, and A. N. Syverud. *J. Phys. Chem. Ref. Data*, 14, 1985.

[48] Ch. Schönenberger. Bandstructure of Graphene and Carbon Nanotubes: An Exercise in Condensed Matter Physics, 2000. http://www.tn.tudelft.nl/tn/Lectures/Meso/meso.htm.

[49] J. Wu, W. Pisula, and K. Mullen. Graphenes as Potential Material for Electronics. *Chem. Rev.*, 107(3):718–747, 2007.

[50] E. Clar. *The Aromatic Sextet.* Wiley, New York, 1972.

[51] S. Okada. Energetics of nanoscale graphene ribbons: Edge geometries and electronic structures. *Phys. Rev. B*, 77(4):041408, 2008.

[52] Y.-W. Son, M. L. Cohen, and St. G. Louie. Energy Gaps in Graphene Nanoribbons. *Phys. Rev. Lett.*, 97(21):216803, 2006.

[53] M. Fujita, K. Wakabayashi, K. Nakada, and K. Kusakabe. Peculiar Localized State at Zigzag Graphite Edge. *J. Phys. Soc. Jpn.*, 65(7):1920–1923, 1996.

[54] K. S. Novoselov. Graphene: Mind the gap. *Nature Mater*, 6(10):720–721, 2007.

A Appendix

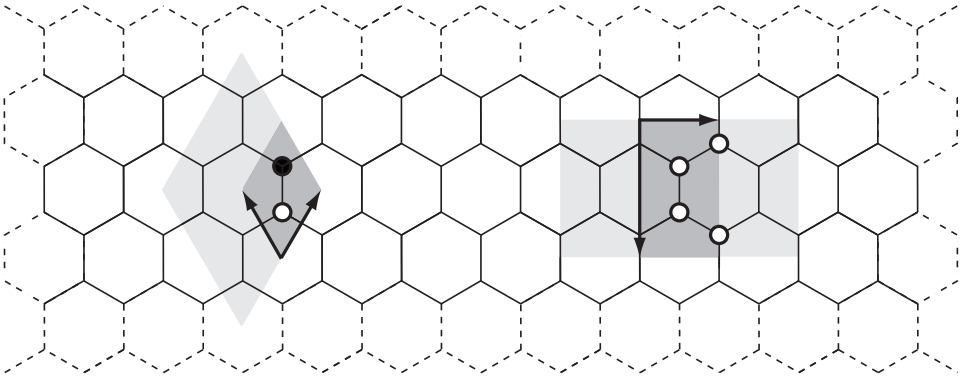

Figure 1: Two unit cells for graphene. On the left side the hexagonal unit cell with two atoms in its basis is shown (dark gray). This is the primitive unit cell. On the right side an orthorhombic cell with four atoms in its basis is presented (dark gray). This cell is more convenient as a starting point for supercell constructions in DFT calculations on GNRs.

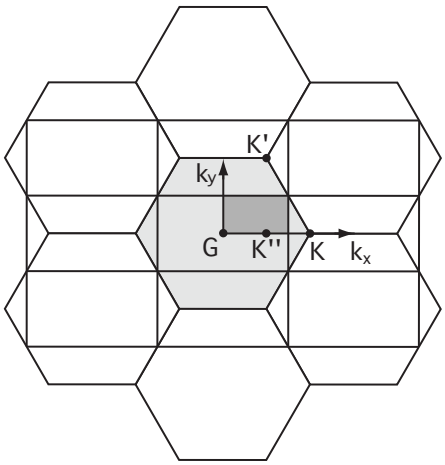

Figure 2: Reciprocal lattice of graphene. If one starts with the hexagonal lattice in real space, also the reciprocal space forms a hexagonal lattice (First Brillouin zone in light gray). In case of the orthorhombic real-space unit cell, the reciprocal space forms an orthorhombic lattice (Because of symmetry, only the area in dark gray has to be studied.). The points where valence and conduction bands meet are situated at the points K and K$'$. By back-folding this point comes to lie at 1/3 on the k_{x} axis in the orthorhombic cell (K$''$).

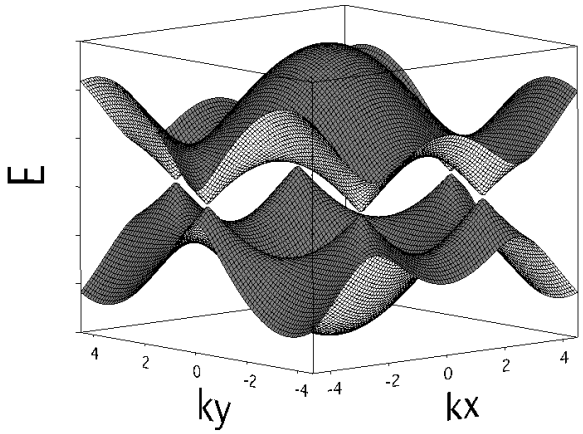

Figure 3: Band structure of graphene calculated in a tight-binding approximation [48]. Notice the conical points where the energy depends linearly on the k-vector. Electrons in this region obey the Dirac equation with the Fermi velocity playing the role of the speed of light [9]. By projecting the bandsurfaces to the k_{x} and k_{y} axes and back-folding to the first Brillouin zone of the orthorhombic lattice, the point K comes to lie at $k_{\mathrm{y}} = 0$ in Fig. 15 and $k_{\mathrm{x}} = 1/3$ in Fig. 16.

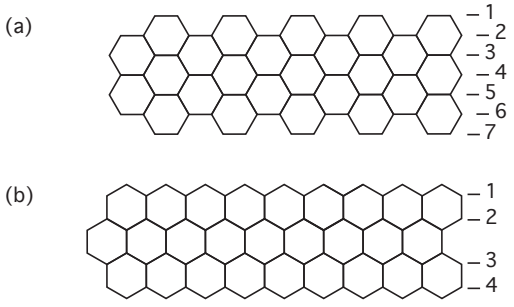

Figure 4: Ribbons with the two fundamental edge geometries and the counting that defines their width. a) Armchair ribbon with width 7 (Notation: 7-AGNR). b) Zigzag ribbon with width 4 (Notation: 4-ZGNR).

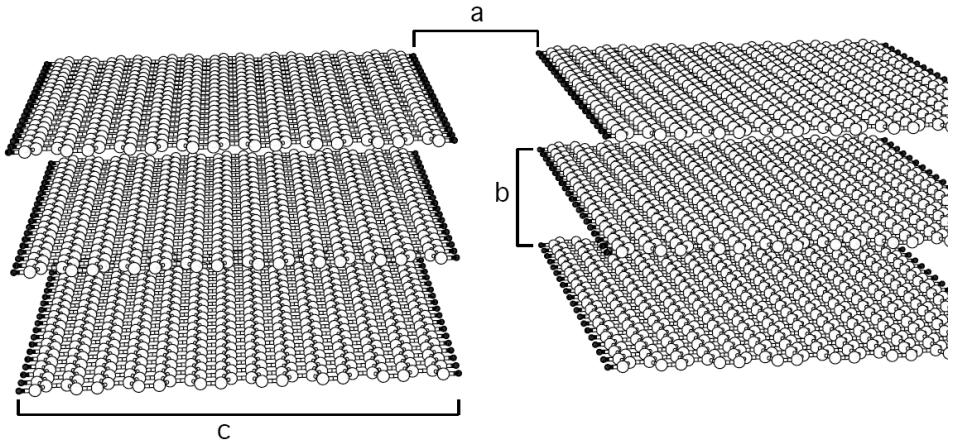

Figure 5: Supercell geometry for DFT calculations. a) in-plane vacuum b) vacuum between planes c) ribbon width.

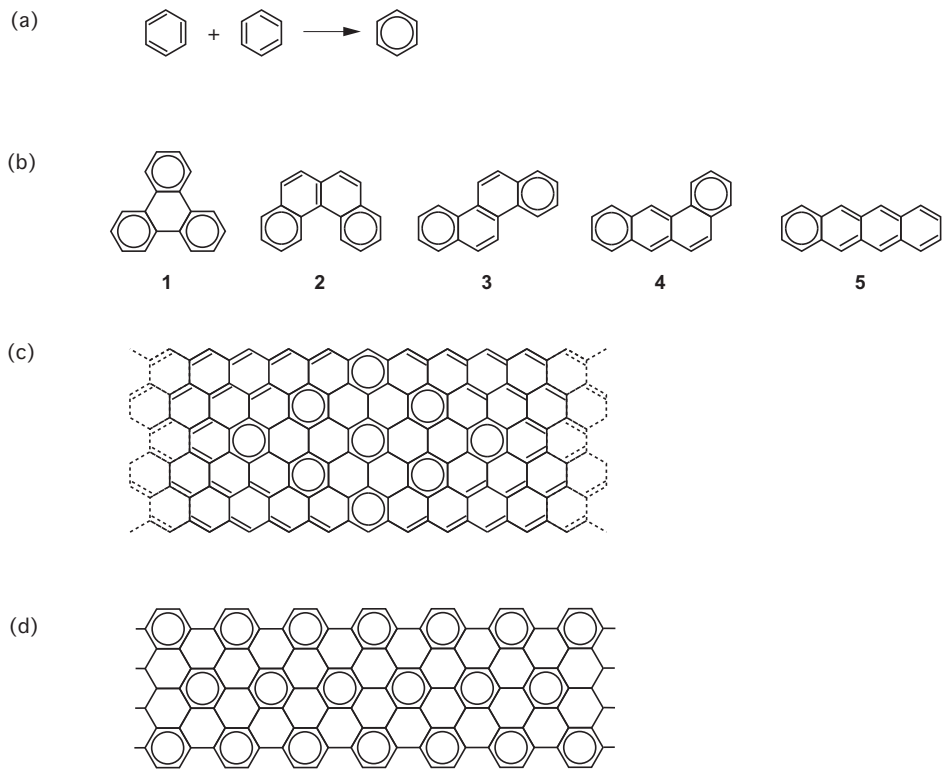

Figure 6: Clar structure analysis. a) The superposition of the two resonant Kekulé structures constituting the aromatic π-sextet ring of benzene is indicated by a solid ring in the Clar structure diagram. Hydrocarbons formed by fusion of benzene hexagons are called polycyclic aromatic hydrocarbon (PAH). These may have aromatic rings and double bonds in their Clar structure diagrams. The stability of a PAH isomer, however, increases with the number of π-sextet rings [49, 50]. If all π-electrons of a PAH are part of an aromatic π-sextet ring, the structure is called all-benzenoid polycyclic aromatic hydrocarbon (PBAH). Graphene is a PBAH. b) The smallest possible PBAH is the tetracyclic triphenylene **1**. Compared with its isomers [4]helicene **2**, chrysene **3**, benz[a]anthracene **4**, and naphthacene **5**, tetracyclic triphenylene is less reactive, more stable and has the largest bandgap [36]. c) The formation of π-sextet rings in monohydrogenated ZGNRs is suppressed. The net structure is quinoidal (two double bonds per hexagon) [36]. Only in the limit of infinite ribbon width the all-benzenoid structure of graphene is restored. ZGNR with different edge-hydrogen decorations may have aromatically more favorable Clar structures, see the manuscript. d) The monohydrogenated 9-AGNR is a perfect PBAH.

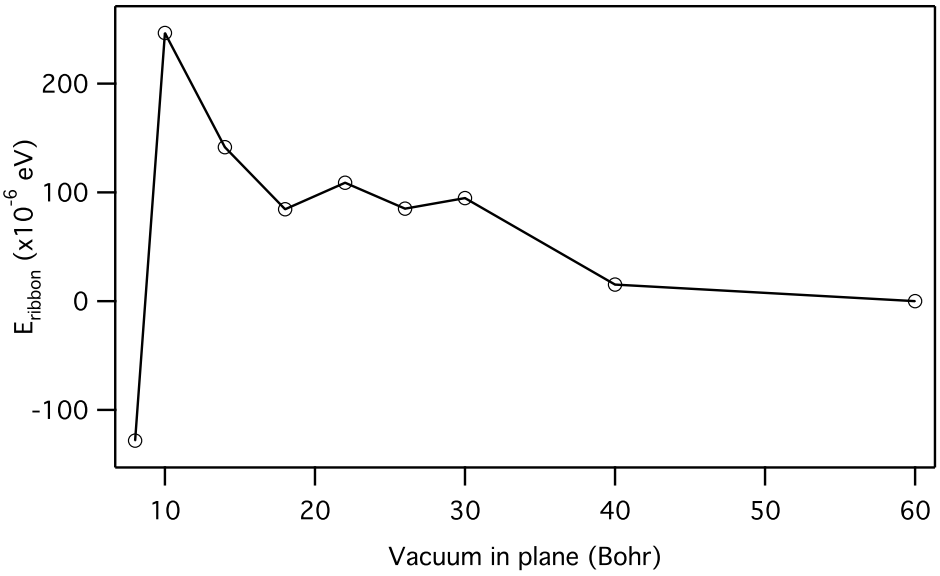

Figure 7: DFT convergence test. Total energy E_{ribbon} versus in-plane vacuum between the ribbons. As reference, the total energy for an in-plane vacuum of 60 Bohr was set to zero.

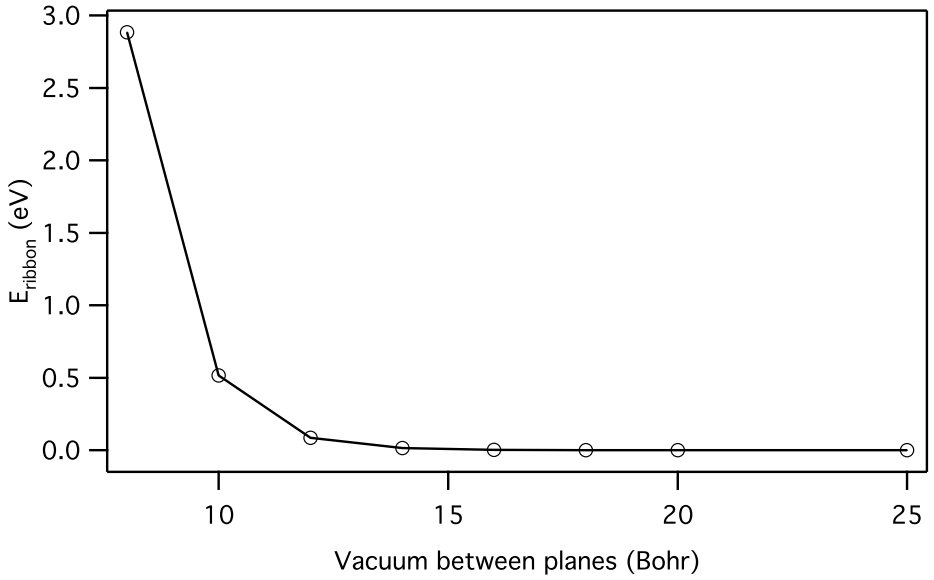

Figure 8: DFT convergence test. Total energy E_{ribbon} versus vacuum dimension between the planes. As reference, the total energy for a vacuum of 25 Bohr was set to zero.

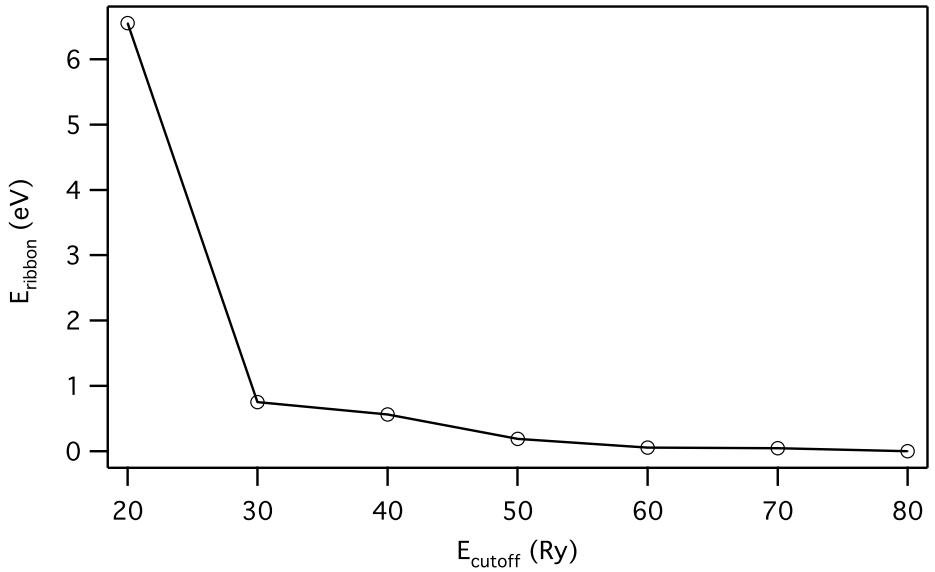

Figure 9: DFT convergence test. Total energy E_{ribbon} versus wave function cutoff energy. As reference, the total energy for $E_{\text{cutoff}} = 80\,\text{Ry}$ was set to zero.

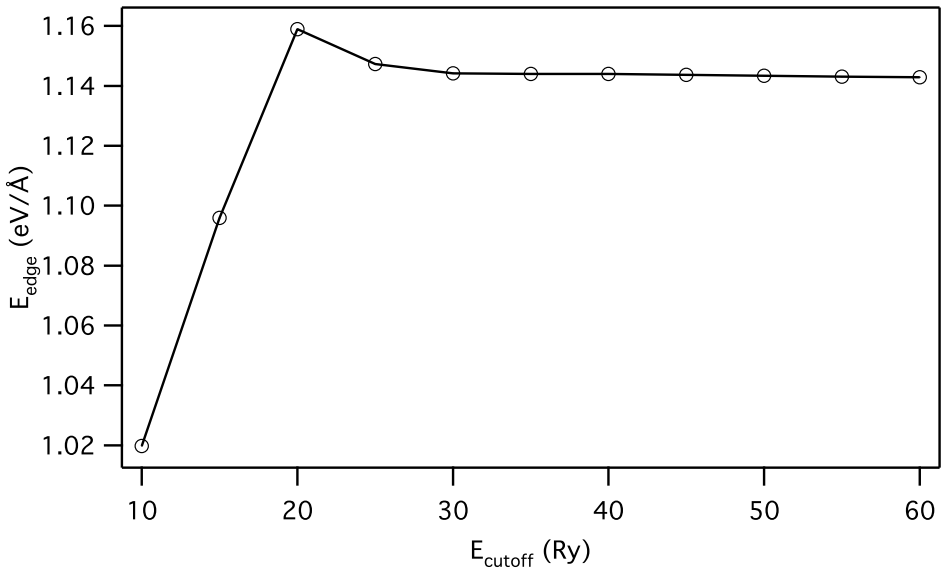

Figure 10: DFT convergence test. Edge energy (at $T = 0$) versus cutoff energy. For the calculation of E_{bulk} and E_{ribbon} the same cutoff energy was used. Note that the edge energy converges earlier than the total energy, Fig. 9.

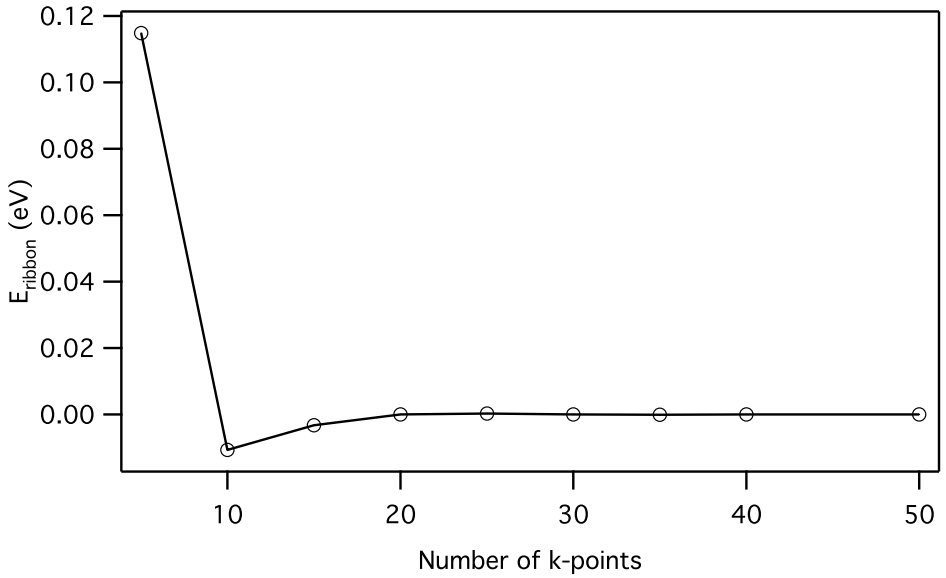

Figure 11: DFT convergence test. Total energy E_{ribbon} versus number of k-points.

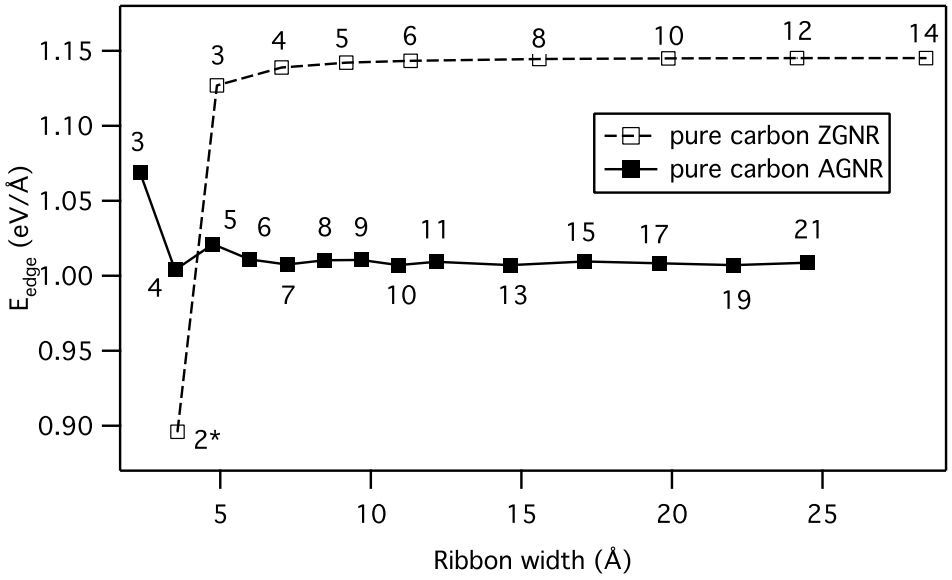

Figure 12: Edge energies (at $T = 0$) of pure carbon GNRs as a function of ribbon width. The numbers besides the data points indicate the width of the ribbons in the notation introduced in Fig. 4. In case of the AGNRs, the edge energy shows a dependence on the ribbon width as it oscillates in a threefold periodicity, see also Fig. 13. *The narrowest ZGNR spontaneously breaks up into two polyyne chains.

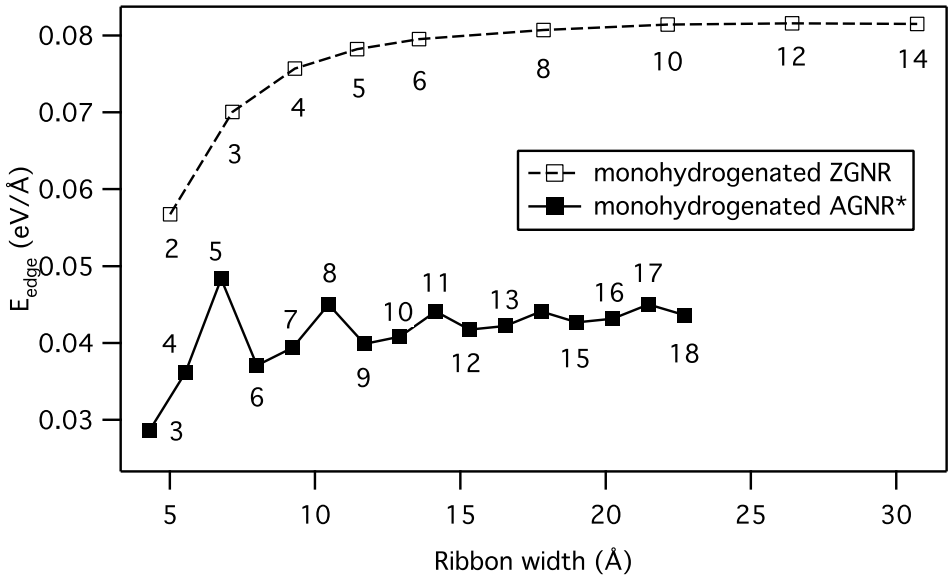

Figure 13: Edge energies (at $T = 0$) of single-hydrogen terminated GNRs as a function of ribbon width. The numbers besides the data points indicate the width of the ribbon. Notice the oscillation in the edge energy of the AGNRs with minima at widths of 3n. *The values for AGNR were taken from [51].

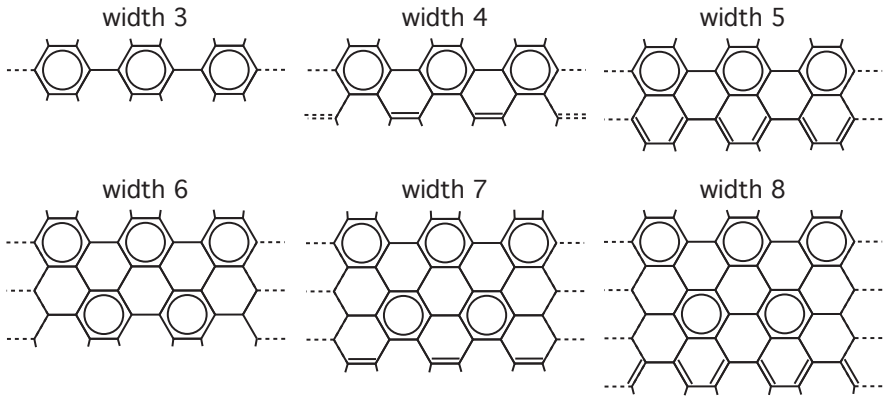

Figure 14: Clar structures of monohydrogenated AGNRs with different widths. The ones with a width of 3n represent PBAHs and are therefore especially stable. In this family the Clar structure is unique, in the other cases different formulations with the same number of rings are possible.

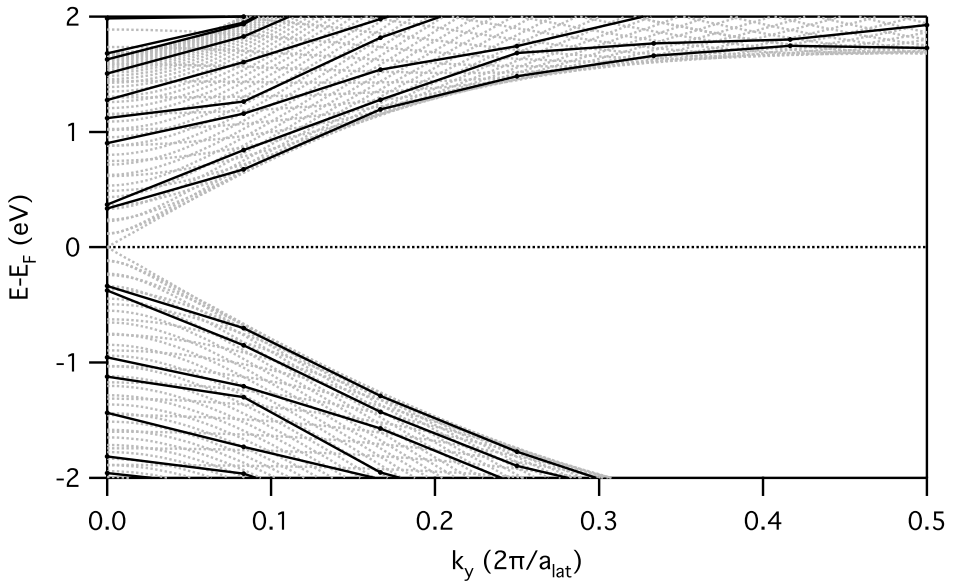

Figure 15: Bandstructure of monohydrogenated 19-AGNR (black) and bulk graphene projected to k_{y} (light gray). The bandgap arises due to quantum confinement and edge effects (bond of outermost carbon atoms is shorter) [52]. The size of the gap varies in a triple periodicity as a function of ribbon width [51, 52].

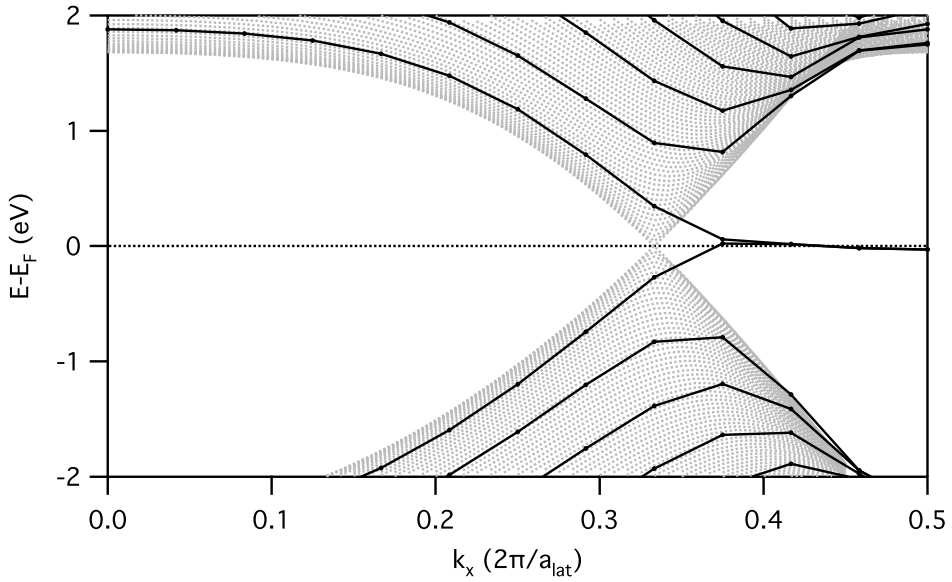

Figure 16: Bandstructure of monohydrogenated 14-ZGNR without spin-polarization (black) and bulk graphene projected to k_{x} (light gray). There is a flat region near the Fermi energy after the K point. This flat region leads to a peak in the density of states around the Fermi energy.

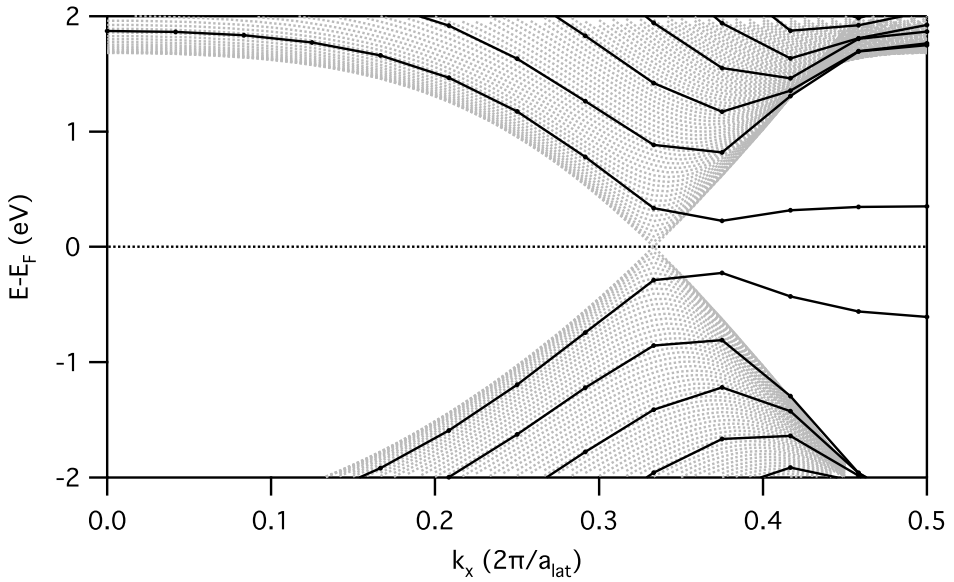

Figure 17: Bandstructure of monohydrogenated 14-ZGNR after spin-polarization is included. A bandgap has opened. The mechanism for the bandgap opening differs from that in the armchair case. The high density of states near the Fermi energy corresponding to the edge states makes spontaneous magnetization through electron-electron interaction possible [53]. In the antiferromagnetic groundstate the two edges show net spin-polarization of different signs, see Fig. 18. The edge atoms on the two sides correspond to the two different atoms in the basis of the hexagonal unit cell, Fig. 1. The symmetry between these sublattices is broken by the magnetization, leading to a bandgap [7, 52, 54].

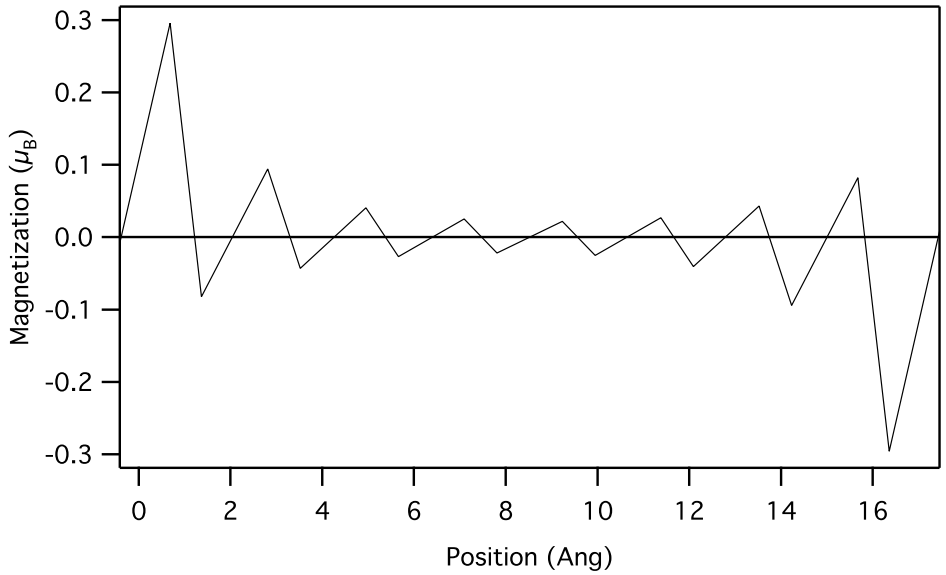

Figure 18: Projected magnetization ($n_\uparrow - n_\downarrow$) versus atom position for 8-ZGNR in the antiferromagnetic groundstate. The edge-hydrogen atoms are not polarized. Most magnetization is found at the outermost carbon atoms.

Stability of Hydrogen Terminated Graphene Ribbons

Tobias Wassmann, Ari P Seitsonen, Marco Saitta, Michele Lazzeri, and Francesco Mauri
IMPMC, Université Paris 6 et 7, CNRS, IPGP, 140 rue de Lourmel, 75015 Paris, France
(Dated: April 11, 2008)

Searching for the most stable configuration of hydrogen-terminated graphene ribbons, we have studied unreconstructed zigzag and armchair strips as well as reconstructions [P. Koskinen et. al., arXiv:0802.2623v1] at different edge-hydrogen densities. To account for realistic experimental conditions, we relate the edge energies from *ab initio* density functional theory calculations to the chemical potential of molecular hydrogen at finite pressure and temperature. The results show that at room temperature and in ambient atmosphere the monohydrogenated armchair ribbon represents the most favorable configuration. The magnetic single-hydrogen terminated zigzag edge becomes stable only at high temperature, low pressure conditions, whereas the most favorable systems in other regions of phase space do not acquire magnetism. In particular, we observed the absence of magnetism in zigzag ribbons at certain edge-hydrogen densities. We discuss the stability of the hydrogenated graphene ribbons in terms of Clar structures.

While two-dimensional graphene [1–5] exhibits fascinating properties such as a light-like dispersion relation for its charge carriers [2] and ballistic transport on large distances [1], its gapless spectrum makes it unsuitable for direct application as channel in field effect transistors (FETs) and other semiconductor devices. Carbon nanotubes (CNTs), the cylindrical form of graphene, on the other hand, have excellent properties for FET applications [6, 7] since—depending on their chirality—a bandgap opens up [8–10] while carrier mobility still remains exceedingly high [11]. Their integration in large-scale circuits represents a serious problem though, and their chirality cannot be controlled during growth [12]. Graphene nanoribbons (GNRs) [13–15] promise to be a valuable alternative to CNTs in this kind of applications [16–18], combining the advantageous electronic properties of CNTs with the possibility of lithographic patterning [17–19].

Among the two fundamental edge geometries in which GNRs appear, zigzag (ZGNR) and armchair (AGNR), in particular the former has caused great resonance in the scientific community. ZGNRs feature magnetism due to two spin-polarized electronic states localized on the edge sites [20] and they possibly turn to half-metal under an external electric field [13, 21]. All this has fired the hope to use ZGNR in future spintronic-devices [13, 22]. The electronic properties of the GNR, however, depend strongly on their width [18], edge geometry [14, 23] and decoration [24]. In particular, the bandstructure approaches the gapless limit of graphene with increasing ribbon width [18, 25, 26]. As a consequence, for semiconductor applications, very narrow ribbons are necessary and it is crucial to control the edge configuration.

Both requirements came a big leap closer to reality with recently reported chemical production of sub 10 nm ribbons with well defined edges [27]. The fast progress made in chemical ribbon derivation motivates the questions of which edge geometry and decoration is energetically most favorable in a given chemical environment and what electronic properties this edge configuration will impose on the ribbon.

We are aware that the relative stability of single-hydrogen terminated [25] and pure carbon [28] GNR with different widths have already been analyzed, even for different hydrogen saturations [26]. These analyses, however, were done at only one single point in the thermodynamical phase space, at absolute zero temperature. In the present work we analyze the stability of carbon nanoribbons at various thermodynamical conditions. From our analysis we can predict which configuration is the most probable one for a given value of hydrogen chemical potential.

To this end we have studied both ZGNR and AGNR with different edge-hydrogen densities. In the case of ZGNR we considered supercells with up to six adjacent hexagons along the ribbon edge. Each of the edge carbon atoms can accomodate up to two hydrogen atoms, allowing to simulate a wide range of hydrogenation states. To distinguish the different configurations we denoted them in the form $\mathrm{zz}(\mathrm{n}_1, \mathrm{n}_2)$ where n_1 stands for the number of consecutive monohydrogenated sites and n_2 the number of double-hydrogen terminated ones. See the drawings in Fig. 1 for some examples of the notation. The zz57(00) system represents a pure carbon edge reconstruction proposed in [29]. The widths of the ZGNR studied here vary from 28.81 Å for zz57(00) to 30.72 Å for zz(1,0).

For the family of AGNRs only the primitive unit cell, consisting of a single column of hexagons, was considered. Again the two edge sites can be saturated with different numbers of hydrogen atoms, referred to by m_1 and m_2 in the form $\mathrm{ac}(\mathrm{m}_1\mathrm{m}_2)$. The edge reconstruction in which the outermost hexagon is reduced to a pentagon [29] is denoted by ac56(m) where m indicates the number of hydrogen atoms bond to the edge site. In this family, the widths of the ribbons lie within 21.48 Å for ac56(0) and 24.12 Å for ac(11). All ribbons examined, armchair and zigzag, have identical edge configurations on both sides.

We used the Quantum-ESPRESSO [30] package to

perform density functional theory (DFT) calculations of the total energies and band structures of the presented systems. A plane wave basis set was utilized for the expansion of the valence wave functions in the generalized gradient approximation [31] to the exchange correlation energy. The core-valence interactions were modeled with Vanderbilt ultrasoft pseudopotentials [32] and a cutoff energy of 30 Ry for the wave functions and 300 Ry for the augmented density was used. The lattice constant was fixed to the experimental value of 2.46 Å [33] but a full relaxation of the atomic positions down to a force threshold of 1 mRy/Å was performed. For the Brillouin zone integration, we employed a uniform k-point sampling with 12 points along the periodic direction for the armchair ribbons and 24, 12, 8, 6, 4, 4 points for the zigzag ribbons with 1, 2, 3, 4, 5, 6 hexagons along the edge in the supercell. In order to model isolated ribbons, we separated them by 9.5 Å vacuum in plane and 8.5 Å between the planes.

The accuracy of the calculations within the above parameters was checked by perfoming some test calculations using a much more accurate parameter set (24 k-points for armchair, 40 for zigzag, cutoff energy 100 Ry, larger separating vacuum). The edge energies in the two sets vary by less than 1.5 meV/Å and we therefore expect the error in our calculations to be at most 3 meV/Å.

We investigate the relative stability of the ribbons using the edge energy, i.e. the formation energy of the edges. In this work the analysis is limited to hydrogen atmosphere. If we denote with E_{ribbon}, E_{bulk} and E_{H_2} the total energies of the ribbon, bulk graphene and H_2 gas and with n_C and n_H the number of carbon respectively hydrogen atoms in the unit cell of the ribbon, the edge energy reads

$$E_{edge} = \frac{1}{2}\left(E_{ribbon} - n_C\frac{E_{bulk}}{2} - n_H\frac{\mu'_{H_2}}{2}\right)\frac{1}{l_{cell}}$$

where $\mu'_{H_2} = E_{H_2} + \mu_{H_2}$ stands for the chemical potential of H_2 on the DFT energy scale and l_{cell} for the length of the unit cell in the direction of the ribbon. E_{bulk} has to be divided by 2 because there are two carbon atoms in the (hexagonal) unit cell of bulk graphene. In the ideal gas approximation and neglecting zero point vibrations, μ_{H_2} can be expressed in thermodynamical quantities as [34, 35]

$$\mu_{H_2} = H^0(T) - H^0(T=0\,K) - TS^0(T) + kT\ln\left(\frac{p}{p^0}\right). \quad (1)$$

Introducing the edge-hydrogen density (per side), $\rho_H = \frac{1}{2}\frac{n_H}{l_{cell}}$ we can rewrite the expression for the edge energy in a form that better reflects the thermodynamics

$$E_{edge} = E^0 - \frac{1}{2}\rho_H\,\mu_{H_2}\,. \quad (2)$$

TABLE I: Edge-hydrogen density and edge energy at absolute zero temperature of all the studied systems.

	ρ_H (Å^{-1})	E^0 (eV/Å)		ρ_H (Å^{-1})	E^0 (eV/Å)
zz(0,1)	0.813	0.2224	ac(22)	0.939	-0.0710
zz(1,1)	0.610	0.0382	ac(21)	0.704	0.2390
zz(2,1)	0.542	0.0119	ac(11)	0.469	0.0321
zz(3,1)	0.508	0.0257	ac(10)	0.235	0.6950
zz(4,1)	0.488	0.0397	ac56(1)	0.235	0.7030
zz(5,1)	0.474	0.0463	ac(00)	0.000	1.0078
zz(1,0)	0.407	0.0809	ac56(0)	0.000	1.4723
zz57(00)	0.000	0.9650			
zz(0,0)	0.000	1.1452			

Here, all DFT energies are combined into

$$E^0 = \frac{1}{2}\left(E_{ribbon} - n_C\frac{E_{bulk}}{2} - n_H\frac{E_{H_2}}{2}\right)\frac{1}{l_{cell}}\,.$$

This quantity represents the edge energy at the absolute zero point.

The values of ρ_H and E^0 for the studied systems are listed in table I. They allow us to find the most stable configuration for a given chemical potential graphically by plotting E_{edge} versus μ_{H_2} via (2). This is done in Fig. 1, however, only the lines corresponding to the most stable ribbons are shown for better readability.

At room temperature the partial H_2 gas pressure in air is $p_{H_2} = 5\times10^{-7}$ bar [35]. This gives a lower limit to the true chemical hydrogen potential, since there are also other hydrogen sources present like water etc. Under these conditions the monohydrogenated AGNR, ac(11), represents the most stable configuration. This structure is already well understood: it is not magnetic and exhibits a band gap of 0.67 eV which compares well with the literature [25].

The configuration with dihydrogenated armchair edges, ac(22), becomes most favorable at very high hydrogen pressures. This ribbon does not show magnetism either. And even though the band structure of the system resembles that of ac(11), Fig. 2, the band gap is significantly smaller, see table II. The important fact to notice here is, that ac(22) represents the most favorable structure with negative edge energy, meaning that spontaneous breaking of graphene into this ribbon becomes possible if the chemical hydrogen potential is higher than -0.133 eV.

Interestingly, there is a small region between the ac(22) and ac(11) where zz(2,1) becomes most stable. In the band structure of this ribbon, the flat bands near the Fermi energy that are typical for zigzag ribbons do not appear and the system consequentially shows no magnetism. In fact, no magnetism was found for the zz(1,1) and zz(3,1) ribbons either. There the band structure features flat edge states near the fermi energy but the flat region is not wide enough to induce a density of states

TABLE II: Bandgaps of the configurations found to be most favorable.

	zz57(00)	zz(1,0)	ac(11)	zz(2,1)	ac(22)
Bandgap (eV)	0.00	0.45	0.67	0.53	0.18

that makes spin polarization favorable. The zz(4,1) and zz(5,1) are magnetic again with the antiferromagnetic state being the most stable one. Later on, we will give a qualitative explanation for the peculiar stability of the zz(2,1) ribbon.

The area where the magnetic monohydrogenated zigzgar ribbon zz(1,0) becomes favorable starts at a point that is quite challenging to reach under experimental conditions. The appearance of pure carbon edges can be excluded even in ultra high vacuum. Of interest is the fact that even though there is an edge state near the Fermi energy appearing in the band structrue of zz57(00), the ground state was found to be not magnetic. This means that the bands at the Fermi energy are already too steep to make spin polarization favorable.

Our analysis of the relative stability of GNR was based

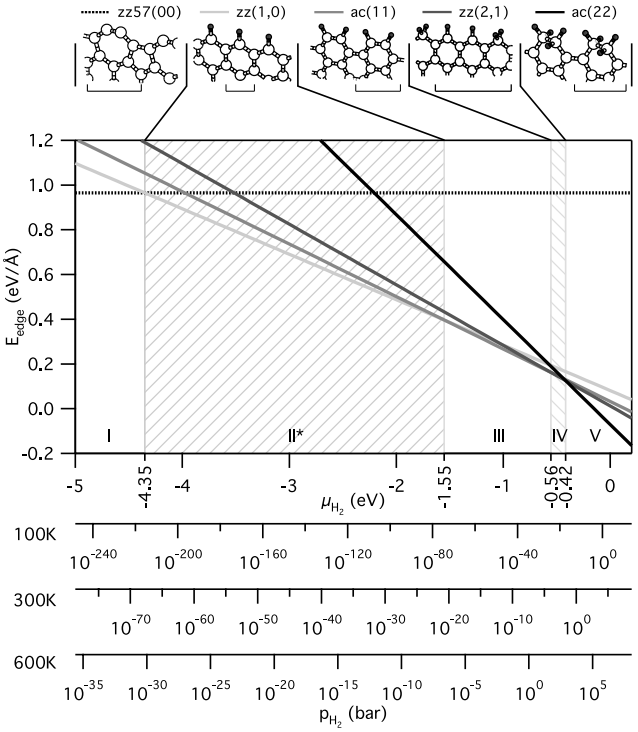

FIG. 1: Edge energies versus μ_{H_2} for the most stable configurations. Magnetism appears only in region II*. The three alternative bottom axis relate the chemical potential at T = 100, 300, and 600 K to the hydrogen pressure via relation (1). The bracket below the schematic drawings of the edges indicates the size of the unit cell.

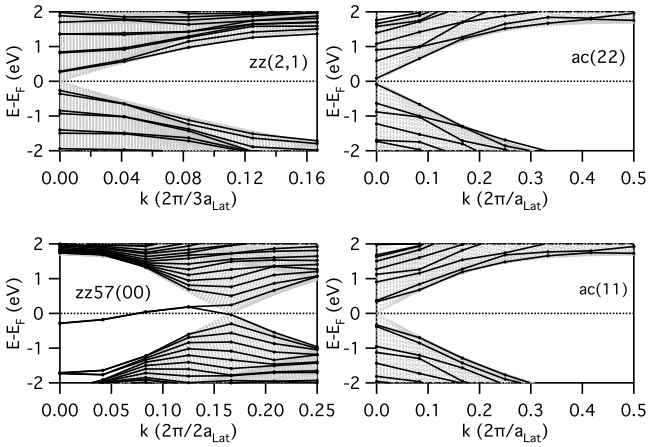

FIG. 2: Band structures of the most stable ribbons and in light gray the one of bulk graphene. For the band structure of the monohydrogenated zigzag ribbon, zz(1,0), we refer to [13, 36–38]. Note that for zz57(00) the bands of a broader ribbon (width 63.40 Å) is shown to see more states in the bulk area.

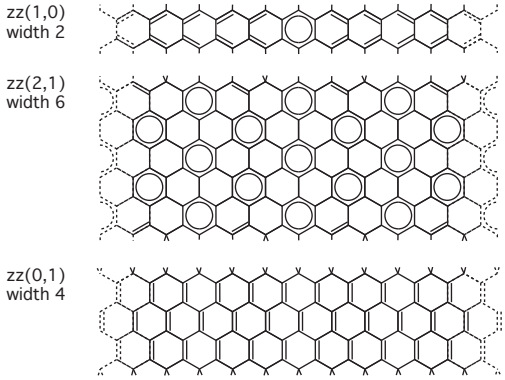

FIG. 3: Clar structures of ZGNRs with different edge-hydrogen densities. While in single-hydrogen terminated, zz(1,0) and double-hydrogen terminated, zz(0,1) ZGNRs aromaticity is suppressed, in the specific configuration of zz(2,1) it is allowed.

on two parameters, the edge-hydrogen density ρ_H and the edge energy at zero temperature, E^0. While the former is a rather obvious quantity, the latter deserves a separate discussion.

In organic chemisty, hydrocarbons consisting of fused benzene hexagons are called polycyclic aromatic hydrocarbons (PAHs) and it is found, that their stability depends on the topological arrangement of the π electrons [39, 40]. Depending on the configuration they can form benzenoid aromatic rings or localized double bonds. For a given PAH system, according to Clar's rule, isomer stability increases with the number of aromatic rings [41, 42]. *All-benzenoid* PAHs (PBAHs) whose total structure can be fully represented by aromatic sextet rings and has no double bonds show particularly high sta-

bility, high melting points and low reactivity [39]. Bulk graphene for instance is a PBAH.

At monohydrogenated zigzag edges the formation of periodic aromatic rings is suppressed as illustrated in Fig. 3. If one hexagon is aromatic, all the others are forced into a quinoidal configuration. This suppression of aromaticity arises at the edges but it forbids aromaticity also on the inside of ZGNR, making them potentially unfavorable. The same holds also for double-hydrogen terminated ribbons, where not even one aromatic circle is allowed.

In the peculiar configuration of zz(2,1), however, the periodic aromaticity of bulk graphene is restored and the ribbon is nearly a PBAH. This edge configuration has the same periodicity as the aromatic sextets and does not disrupt them. The resulting high degree of aromaticity is reflected by the fact that zz(2,1) has the lowest edge energy at zero temperature of all the zigzag ribbons that we examined. In configurations with other edge periodicity as zz(1,1), zz(3,1), zz(4,1), and zz(5,1), some aromatic rings with the periodicity of the edge are allowed, this periodicity however collides with the intrinsic scheme of aromatic rings.

Single- and double-hydrogen terminated armchair edges both are compatible with periodic aromatic rings whereas asymmetrically passivated edges such as ac(21) interfere with them. In this context it is remarkable that also the giant benzenoids described lately have mainly armchair edges [40].

Although the analysis in terms of Clar structure has a pure qualitative character we found it to reproduce a good part of the energy characteristics of hydrogenated GNR and used it as a guideline in our search for favorable structures.

In conclusion, we have performed *ab initio* DFT calculations on GNR with different hydrogen-terminated edge configurations to study their relative stability as a function of the hydrogen chemical potential. According to our analysis, at room temperature and ambient pressure, the monohydrogenated AGNR represents the most stable configuration. In the region of very high hydrogen pressure, the double-hydrogenated AGNR exhibits the lowest edge energy. Between the two kinds of armchair ribbons, there is a region where a ZGNR configuration in which every third edge atom is double-hydrogen terminated becomes favorable. This structure—in contrast to single– or double-hydrogen therminated ZGNR—does not feature magnetism. Its particular stability is explained by the high degree of aromaticity of the structure. The much discussed magnetic, single-hydrogen terminated ZGNRs are likely only at very low hydrogen chemical potentials. We are excited to see our predictions tested in actual experiments.

[1] K. S. Novoselov et al., Science **306**, 666 (2004).
[2] K. S. Novoselov et al., Nature **438**, 197 (2005).
[3] Y. Zhang et al., Nature **438**, 201 (2005).
[4] A. K. Geim and K. S. Novoselov, Nat Mater **6**, 183 (2007).
[5] M. I. Katsnelson, Materials Today **10**, 20 (2007).
[6] S. J. Tans et al., Nature **393**, 49 (1998).
[7] P. Avouris, Acc. Chem. Res. **35**, 1026 (2002).
[8] N. Hamada et al., Phys. Rev. Lett. **68**, 1579 (1992).
[9] R. Saito et al., Appl. Phys. Lett. **60**, 2204 (1992).
[10] M. S. Arnold et al., Nat Nano **1**, 60 (2006).
[11] S. Frank et al., Science **280**, 1744 (1998).
[12] P. McEuen et al., IEEE Trans. Nanotechnol. **1**, 78 (2002).
[13] Y.-W. Son et al., Nature **444**, 347 (2006).
[14] K. Nakada et al., Phys. Rev. B **54**, 17954 (1996).
[15] C. Berger et al., Science **312**, 1191 (2006).
[16] B. Obradovic et al., Appl. Phys. Lett. **88**, 142102 (2006).
[17] Z. Xu et al., Appl. Phys. Lett. **90**, 223115 (2007).
[18] M. Y. Han et al., Phys. Rev. Lett. **98**, 206805 (2007).
[19] C. Berger et al., J. Phys. Chem. B **108**, 19912 (2004).
[20] A. Yamashiro et al., Phys. Rev. B **68**, 193410 (2003).
[21] E.-J. Kan et al., Appl. Phys. Lett. **91**, 243116 (2007).
[22] O. V. Yazyev and M. I. Katsnelson, Phys. Rev. Lett. **100**, 047209 (2008).
[23] D. Gunlycke et al., Appl. Phys. Lett. **90**, 142104 (2007).
[24] D. Gunlycke et al., Appl. Phys. Lett. **91**, 112108 (2007).
[25] S. Okada, Phys. Rev. B **77**, 041408 (2008).
[26] V. Barone et al., Nano Lett. **6**, 2748 (2006).
[27] X. Li et al., Science **319**, 1229 (2008).
[28] T. Kawai et al., Phys. Rev. B **62**, R16349 (2000).
[29] P. Koskinen et al. (2008), arXiv:0802.2623v1.
[30] P. Giannozzi et al., URL `http://www.quantum-espresso.org`.
[31] J. P. Perdew et al., Phys. Rev. B **46**, 6671 (1992).
[32] D. Vanderbilt, Phys. Rev. B **41**, 7892 (1990).
[33] P. Trucano and R. Chen, Nature **258**, 136 (1975).
[34] K. Reuter and M. Scheffler, Phys. Rev. B **65**, 035406 (2001).
[35] C. Bailey et al. (2007), URL `http://epubs.cclrc.ac.uk/work-details?w=40553`.
[36] L. Pisani et al., Phys. Rev. B **75**, 064418 (2007).
[37] Y. et al. Li, Phys. Rev. Lett. **99**, 186801 (2007).
[38] Y.-W. Son et al., Phys. Rev. Lett. **97**, 216803 (2006).
[39] J. Wu et al., Chem. Rev. **107**, 718 (2007).
[40] M. Watson et al., Chem. Rev. **101**, 1267 (2001).
[41] E. Clar, *Polycyclic Hydrogarbons* (Academic Press, London, 1964).
[42] E. Clar, *The Aromatic Sextet* (Wiley, New York, 1972).